Journal of Applied Fluid Mechanics, Vol. 9, No. 6, pp. 3033-3043, 2016.
Available online at www.jafmonline.net, ISSN 1735-3572, EISSN 1735-3645.

Numerical Simulation of Coolant Temperature Rise by Copper Metal foam Insert in Water-cooled Air-Kerosene Combustion Gas Heated Cooling Channel

J. B. Ralphin Rose[1†], S. K. George[1] and K. Rashid[2]

[1] *Department of Aeronautical Engineering, Anna University, Tirunelveli, Tamil Nadu, 627007, India*
[2] *Thermal Engineering Group, Liquid Propulsion Systems Centre, ISRO, Trivandrum, 695547, India*

†*Corresponding Author Email: bruceralphin@gmail.com*

(Received February 12, 2015; accepted January 6, 2016)

ABSTRACT

In the present article, the application of copper metal foam in the cooling channels of a water cooled air-kerosene combustion gas heated test bench model that partially recreates a section of liquid rocket motor cooling system is numerically simulated. It helps to study the influence of copper metal foam inserts on coolant temperature rise, pressure and velocity. In the first case, the problem of conjugate heat transfer from the test bench to the coolant without copper metal foam is analyzed using coupled CFD analysis in ANSYS work bench. Subsequently, a second micro-analysis is conducted by introducing a single cell of heated copper foam into the coolant using the results obtained from the first case. This micro-analysis is repeated for different flow velocity magnitudes of the coolant inlet flows. The results show positive contribution in the overall temperature rise of the coolant. Additionally, the micro-analysis also shows that, as the velocity of coolant increases the overall temperature rise of the coolant decreases and the results are presented here graphically.

Keywords: CFD; Copper metal foam; Open cell metal foam; Heat transfer analysis.

1. INTRODUCTION

Modern liquid rocket motors are mostly regenerative cooled, and uses milled rectangular cooling channels as heat exchangers. This arrangement actively cools the engine from extreme temperature produced by the combustion gases thereby allowing the engine to operate within safe thermal limits. The coolant is often being the fuel, oxidizer or a mixture of both gets preheated during the cooling process. It is then fed into the combustion chamber through the injector causing effective combustion of the fuel-oxidizer mixture. In addition to the Regenerative Cooling (RC) technique, rocket engine often employ other cooling techniques such as film cooling, transpiration cooling however these techniques are expensive owing to the fact that it causes at least some portion of the fuel to pass through the combustion chamber and throat section of the engine without positively contributing to overall thrust.

Copper metal foam is an advanced material having excellent properties such as high thermal conductivity, high porosity, low density, good strength and is used in applications involving heat exchanging anywhere from industrial power generation plants to electronics. Even slight enhancement of RC without adding much weight or production cost results in improved efficiency, enhanced life of rocket motor, ultimately helps carry more pay load which means more profit. In this article, the thermal effects on coolant temperature while introducing copper metal foam inside the cooling channel of an air-kerosene combustion gas passed test bench model is numerically simulated in two co-dependent cases. The coupled CFD analysis is preferred as a solution method to investigate the influence of Copper metal foam in the regenerative cooling process.

2. BACKGROUND

The heat transfer performance in metal foams has gained much focus under natural and forced convection techniques. It has been experimentally and theoretically studied often in

the past decades using a multitude of fluids. Ding *et al.* (2011) conducted an experimental study in copper foam equipped heat exchanger and concluded that involvement of copper foam greatly increases the heat transfer coefficient. Bai and Chung (2011) also performed a numerical investigation in heat exchangers with copper foams and concluded the similar findings. Hunt and Tien (1988) assumed local thermal equilibrium and studied thermal dispersion effects on forced convection in metal foams using water as fluid phase. They determined that the conduction of metal foams may not be significant because of its thin cell ligaments, and dispersion dominates the heat transport for metal foams with high porosity.

Pressure drop and heat transfer characteristics of FeCrAlY as well as copper foams with different relative density and cell size were examined experimentally by Zhao *et al.* (2002, 2004). The results indicate that heat transfer of FeCrAlY samples is more sensitive to its relative density than the pore size while in copper samples the effect of relative density was less significant compared to its cell size. It is because of different thermal resistances on the solid side for FeCrAlY and copper samples. Electrically heated Aluminum and copper foam samples of 5, 10, 20 and 40 pores per inch (ppi) and different porosities were investigated with forced air convection by Mancin *et al.* (2012, 2011). Their results exhibited that both the surface area and foam finned surface efficiency played a crucial role in the entire heat transfer performance. It was also observed that the heat transfer coefficient increases with mass flow rate of air and the pressure drop increases with pore density.

Pressure drop and heat transfer in the compressed aluminum foams using water as coolant was studied by Boomsma and Poulikakos (2001, 2002) and the effect of compression on the hydraulic characteristics and heat transfer were examined. Their results illustrated that the pre-compression porosity had a little effect on the final permeability and foam coefficient. Similarly, the permeability and overall hydraulic behavior of the compressed foams is determined by the post-compression porosity. When compared to the commercially used heat exchangers, the metal foam heat exchanger shows a favorable reduction in thermal resistance, and hence a better heat transfer performance is achieved.

Odabaee *et al.* (2011, 2012) performed a numerical study for examining the heat transfer from a metal foam-wrapped solid cylinder and tube bundle. Their crucial observation is that the porous layer thickness will be an essential factor that determines the increase in heat transfer and pressure drop. Odabaee and Hooman (2011) conducted an optimization design of metal foam heat exchangers in air-cooled condensers of a geothermal power plant based on first as well as second law of thermodynamics. It was concluded that, while the former aimed for the highest heat transfer rate with as much low pressure drop as possible, the latter minimized the entropy that was generated in the thermodynamic system. Ultimately, both methods led to the same optimal design. Heat transfer performance of tubes that are covered externally with metal foam was compared with helically finned tubes through experimental investigation by T'joen *et al.* (2010). The metal foam covered tubes with small tube spacing and small foam heights offer significant benefits at air velocity greater than 4 m/s when a good metallic bonding between the foams and the tubes is achieved. The bonding thermal resistant has been calculated to demonstrate their strong impact. Analysis on double tube metal foam filled heat exchangers was conducted by Lu *et al.* (2006) and Zhao *et al.* (2006) and the analytical solutions are obtained subject to some assumptions. The results highlighted superior performance of metal foam heat exchangers when compared to conventional finned tube heat exchangers.

3. COOLING CHANNEL TEST BENCH ANALYSIS (CASE: 1)

The cooling channel test bench assembly is designed to partially recreate a section of the liquid rocket model. Its general arrangement and dimension is shown in Fig.1 (All dimensions are in mm). The three dimensional (3D) isometric view of the assembly designed using CATIA software is shown in Fig. 2. Geometric scaling may be modified for the experimental set up as per the mass flow requirements in a later stage. The values of interest such as global temperature and pressure in the cooling channel are observed to confirm that they reach a steady state. Residual RMS Error values are maintained above 10^{-4} for all variables and the overall imbalance is below 1%.

3.1 Modeling

The test bench is modeled using CATIA V5 R20 software tool. The complex geometry of the assembly has been eliminated and a simplified version is used for the purpose of analysis. It has three domains namely Coolant, Cooling channel and combustion gas. All the domains are modeled as independent parts and subsequently assembled in CATIA assembly work bench. The assembly is then converted to a step file format and exported to ANSYS workbench toolkit for further analysis.

3.2 Meshing

The 3D meshing is done using Gambit module which is a part of FLUENT code. The meshed geometry contains 6, 84,789 nodes and 23, 29,194 elements. In order to capture the flow field and heat transfer characteristics near the walls precisely up to 9 inflation layers are created with a first layer of height 1×10^{-4} m at a growth rate of 1.2. It helps to visualize the temperature changes near the contact regions with high order of accuracy. The image of the mesh from various section planes are shown in Fig. 3 and Fig. 4.

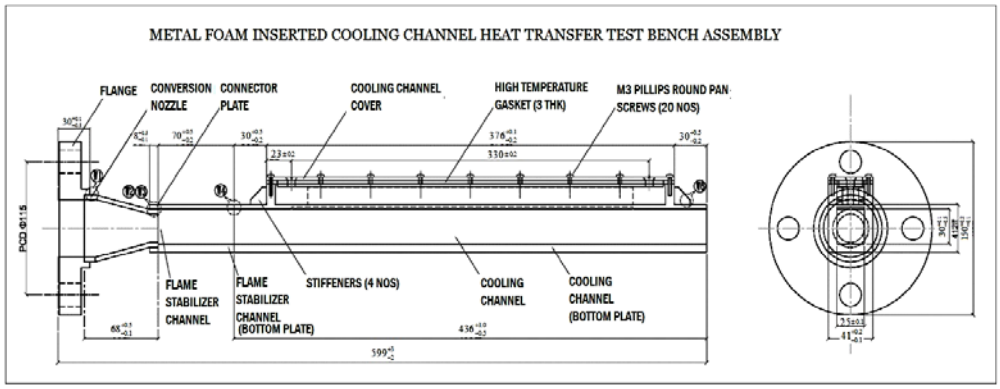

Fig. 1. General arrangement drawing of cooling channel test bench.

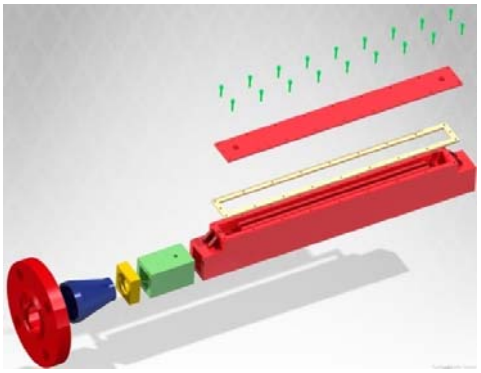

Fig. 2. 3-D model of cooling channel test bench.

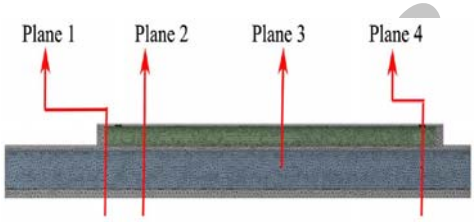

Fig. 3. Longitudinal cut section of test bench with mesh details.

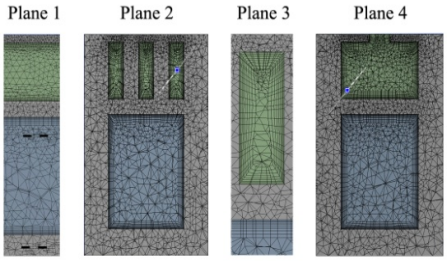

Fig. 4. Cross-section of test bench with mesh details.

3.3 Mesh Independency Study

Mesh independency is studied for two different grid resolutions to ensure its negligible influence in the results. The following 3-step process was used for the grid independence study: 1). Initial simulation is done with 1 million cells and convergence of residual error with values of interest is monitored (imbalances below 1%). 2). The convergence criterion was not attained through step-1 and the number of cells has been increased to 2.5 million in step-2. It is observed that the residual error drops below 10^{-4} and the monitor points are steady after few hundreds of iterations. 3). Again the number of cells has been increased to 3.5 million and the simulation results are converged with residuals less than 10^{-5}. However, the monitor values of interest obtained in step-2 are within the allowable tolerance for the mesh resolution in step-3. Therefore, it is concluded that further refinement in mesh wouldn't influence the simulation results significantly but it increases the run time (Kherief *et al.* 2014). The residual convergence plot history corresponding to step-2 and step-3 are presented in Fig. 5 and Fig.6 respectively.

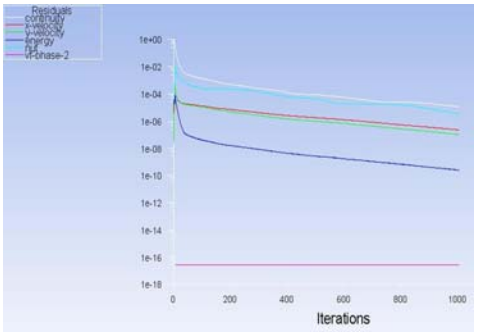

Fig. 5. Residual convergence for step-2.

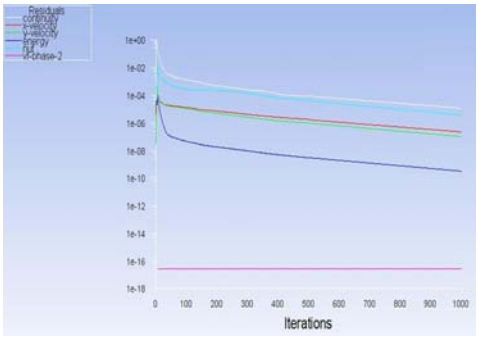

Fig. 6. Residual convergence for step-3.

Table 1 Material/Fluid properties used in test bench analysis

Material / Fluid	Density (Kg/m^3)	Specific Heat (J/Kg-K)	Thermal Conductivity (W/M-K)	Viscosity (Kg/M-s)
Coolant (Water)	998.2	4182.00	0.60	0.001003000
Air-Kerosene Combustion Gas	Ideal Gas	1178.00	0.07992	0.000047154
Cooling Channel (SS321)	8030	502.48	22	-

Table 2 Boundary condition used in test bench analysis

Sl.No	Domain	Magnitude (m/s)	Gauge Pressure (Pa)	Temperature (K)	Backflow Direction Method	Inlet / Outlet Type
1	Coolant Inlet	0.90	101350	300.00	Normal to Boundary	Velocity Inlet
2	Coolant Outlet	-	101325	300.00	Normal to Boundary	Pressure Outlet
3	Combustion Gas Inlet	-	300000	1073.15	Normal to Boundary	Pressure Inlet
4	Combustion Gas Outlet	-	101325	300.00	Normal to Boundary	Pressure Outlet

Post grid independency study has revealed the fact that the monitor points are steady even after enhancing the grid points about 1 million. The above procedure was repeated several times to ensure the mesh refinement for the required solutions. Finally, the smallest mesh corresponding to the Fig .5 is utilized for the simulation because of less simulation run time and optimum accuracy. Solution is converged with imbalances below 1% (stability of the monitor values) for pressure and coolant temperature contours as the number of iterations reaches about 1200. The required CPU time to reach the solution convergence for each input condition is 1 hour 22 minutes.

3.4 Setup and Boundary Conditions

The combustion gas inlet and outlet, coolant inlet and outlet planes are shown in Fig.7. The properties of material/fluid and boundary conditions are given in Table 1 and Table 2 respectively. Laminar flow and viscous heating conditions are used for the present foam and coolant analysis in ANSYS.

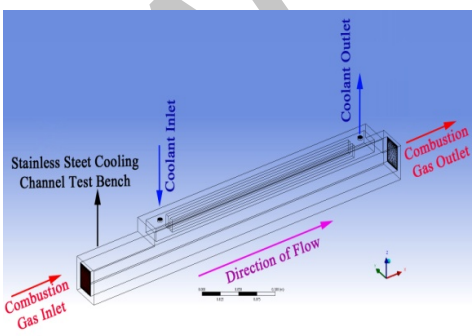

Fig. 7. Inlet and outlet planes of the test bench.

4. METAL FOAM MICRO-ANALYSIS (CASE: 2)

Copper metal foams are cellular structures forming an open interconnected network made of solid copper metal. It has become one of the most promising materials for thermal applications because of its high surface area to volume ratio, stiffness, strength and can be processed in large quantities at a low cost. Enhanced flow mixing (convection) is achieved because of the tortuosity of metal foams. It can be manufactured in different thickness and ppi according to the requirements. Fig. 8 shows copper foam of different thickness and ppi manufacture by Nanoshell LLC in United States.

Fig. 8. Copper metal foams of various thickness and ppi.

4.1 Geometry of Metal Foam

The typical micro structure of open cell metal foam is assumed to be made of ligaments that form a network of interconnected Tetra- kai-Decahedron (TD) cells. The TD cell (displayed in Fig. 9) consists of six squares and eight hexagons and was first published in the Philosophical Magazine by Lord Kelvin (1887). The TD cell is an idealized shape that is most likely be attained in the metal foam from the nature of foaming process and is indicated by D'Arcy (1995).

A 50 ppi and 3 mm thick copper foam (by Nanoshell LLC, United States) is microscopically examined using a Baty Venture 2510 AB3-V Vision system and the images obtained directly from the equipment is shown in Fig. 9. It is observed that the average diameter of a unit cell is 1.3 mm and the diameter of the ligament is 0.15

mm. The images also confirm that the shape of the unit cell is consistent with the Lord Kelvin's Tetra-kai-Decahedron model as presented in Fig. 10.

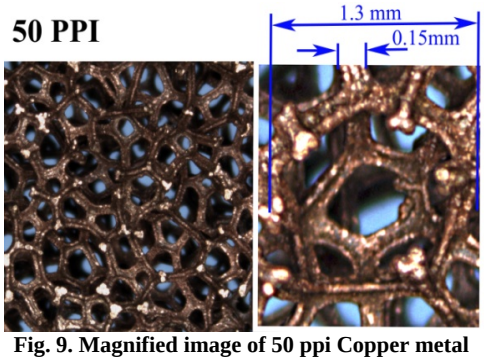

Fig. 9. Magnified image of 50 ppi Copper metal foam with dimensions.

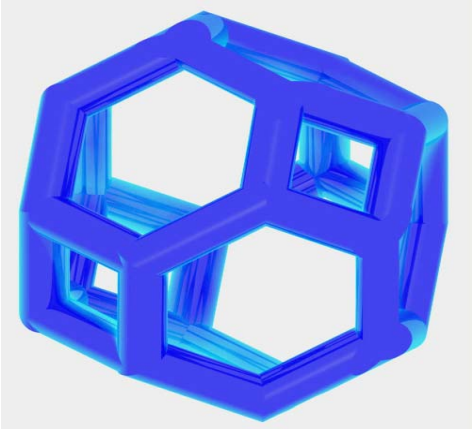

Fig. 10. 3-D model of Tetra-kai-Decahedron cell.

4.2 Modeling

The model consists of two domains: Primarily, a TD unit cell of the copper foam (solid domain) modeled based on the dimensions that are obtained from the microscopic examination of copper metal foam shown in Fig. 9. Next, the surrounding coolant (Liquid domain) consists of a square cross-section of sides with 1.3 mm and having a total length of 8 mm. Both the domains are modeled as independent parts and later assembled using CATIA tool. The assembled sections are then converted into a step file format and exported to ANSYS work bench for analyzing the flow characteristics.

3.3 Assumptions in Metal Foam Micro Analysis

The metal foam micro analysis is done as an extension to the cooling channel test bench analysis. Based on the results obtained from cooling channel test bench analysis, it is observed that the Stainless Steel (SS321) wall which separates the combustion gas domain and the coolant domain is having an average temperature of 550 K.

It is assumed that after the insertion of metal foam into the cooling channel, the bottom cells of the foam which are in direct contact with SS321 separation wall will be at thermodynamic equilibrium because of the conduction. Hence, the temperature is also maintained at 550 K and the justification for this assumption is clearly illustrated in Fig. 11. Based on this assumption, the TD unit cell is defined as solid copper kept at a constant temperature of 550 K during the analysis.

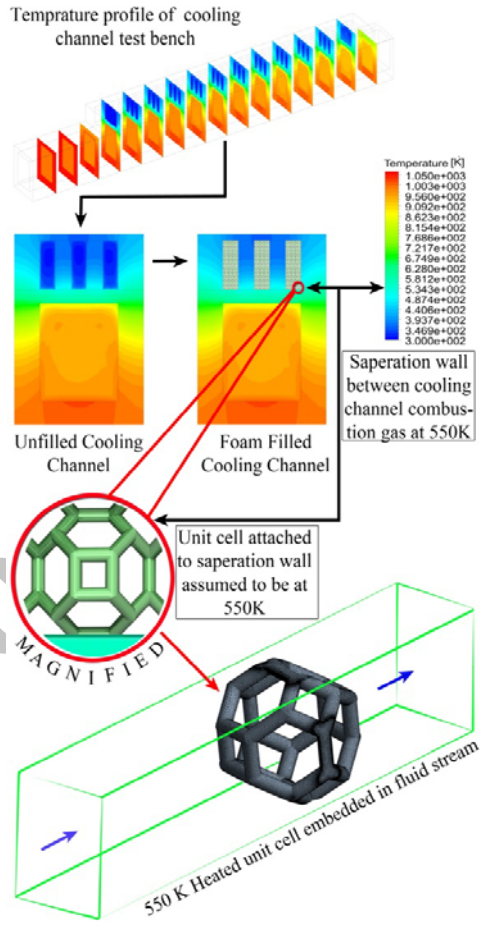

Fig. 11. Illustration justifying the assumption in metal foam micro analysis.

4.4 Meshing

The 3D meshing is done using Gambit module that is similar to cooling channel test bench analysis. The mesh contains 3, 55,205 nodes and 20, 11,883 elements. In order to capture the flow effects and heat transfer near the walls and contact regions, up to 6 inflation layers are created with a first layer height of 1 $x10^{-4}$ m at a growth rate of 1.2 surrounding the foam. A fine mesh is also given to the fluid region immediately surrounding the unit cell of foam to capture the thermal and flow characteristics in the coolant. The mesh details from various section planes are highlighted in Fig. 12.

4.5 Setup and Boundary Conditions

A schematic view of coolant inlet, coolant outlet and embedded unit cell of the copper metal foam is shown in Fig. 13. The coolant is defined as liquid

Table 3 Material/Fluid properties used in metal foam micro analysis

Material / Fluid	Density (Kg/m^3)	Specific Heat (J/Kg-K)	Thermal Conductivity (W/M-K)	Viscosity (Kg/M-s)
Coolant (Water)	998.2	4182.00	0.60	0.001003000
Copper Foam (Unit Cell)	8978	381.00	387.60	-

Table 4 Boundary condition used in metal foam micro analysis

Sl.No	Domain	Magnitude (m/s)	Gauge Pressure (Pa)	Temperature (K)	Backflow Direction Method	Inlet/Outlet Type
1	Coolant Inlet	0.90	101350	300.00	Normal to Boundary	Velocity Inlet
2	Coolant Outlet	-	101325	300.00	Normal to Boundary	Pressure Outlet
3	Coolant Inlet	1.00	101350	300.00	Normal to Boundary	Velocity Inlet
4	Coolant Outlet	-	101325	300.00	Normal to Boundary	Pressure Outlet
5	Coolant Inlet	1.50	101350	300.00	Normal to Boundary	Velocity Inlet
6	Coolant Outlet	-	101325	300.00	Normal to Boundary	Pressure Outlet
7	Coolant Inlet	2.00	101350	300.00	Normal to Boundary	Velocity Inlet
8	Coolant Outlet	-	101325	300.00	Normal to Boundary	Pressure Outlet
9	Coolant Inlet	2.50	101350	300.00	Normal to Boundary	Velocity Inlet
10	Coolant Outlet	-	101325	300.00	Normal to Boundary	Pressure Outlet
11	Coolant Inlet	3.00	101350	300.00	Normal to Boundary	Velocity Inlet
12	Coolant Outlet	-	101325	300.00	Normal to Boundary	Pressure Outlet
13	Coolant Inlet	3.50	101350	300.00	Normal to Boundary	Velocity Inlet
14	Coolant Outlet	-	101325	300.00	Normal to Boundary	Pressure Outlet

water and the TD unit cell is defined as solid copper with a constant temperature of 550 K as illustrated in Fig. 11. The properties of materials/fluid and boundary conditions for the analysis are given in Table 3 and Table 4 respectively.

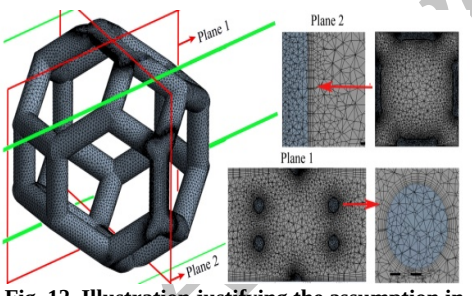

Fig. 12. Illustration justifying the assumption in metal foam micro analysis.

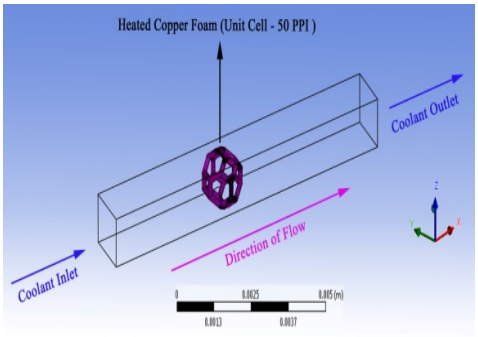

Fig. 13. Inlet and outlet planes of metal foam micro analysis.

5. RESULTS AND DISCUSSION

5.1 Results of Test Bench Analysis

The Fig 14 (a) shows the global temperature profile of the coolant, cooling channel and combustion gas domain at various cross-sections along the x-axis. It indicates the transfer of heat from the combustion gas domain through the stainless steel cooling channel domain into the coolant domain (Lebedev *et al.* 2009). A more detailed local temperature profile of the coolant domain is displayed in Fig 14 (b). In the same fashion, the global pressure at various cross sections in coolant and combustion gas domain is presented in Fig 15 (a). Subsequently, the local pressure at various cross sections in coolant domain is shown in Fig 15 (b) and the results are consistent with the temperature contours.

The coolant is absorbing heat from the cooling channel thus raising its temperature from 300 K at inlet to 365 K outlet during its transit through the cooling channel as illustrated in Fig. 16. It also indicates that the temperature of the stainless steel cooling channel (separation wall) remains at an average of 550 K which clearly supports the assumption used in the metal foam micro analysis illustrated in Fig. 11.

5.2 Results of Metal foam Micro Analysis

The Fig 18, Fig 19. Fig. 20, show the temperature profile, pressure and velocity graphically in the YX and XZ plane of the coolant as it passes through the TD unit cell of the foam at 1.0 m/s. The Fig. 21 shows plot of temperature v/s location of coolant indicating the gradual rise in temperature of the coolant as it passes through the TD unit cell at

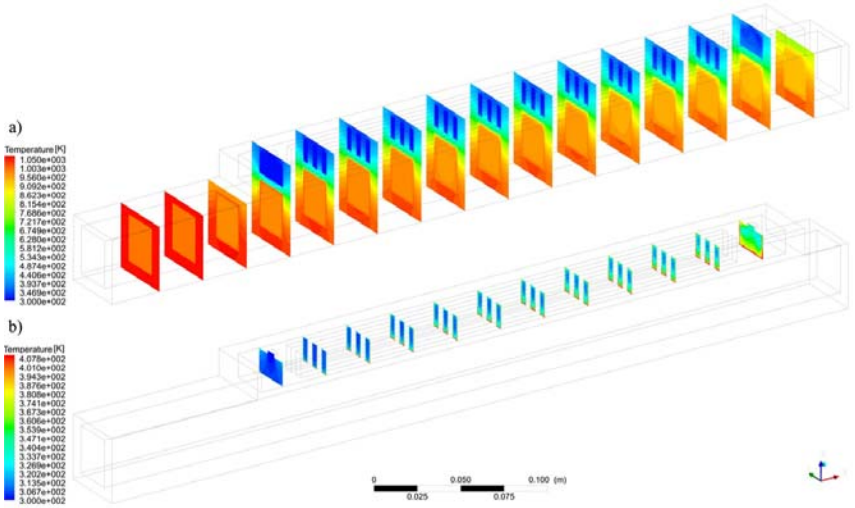

Fig. 14. (a): Global Temperature profile at various cross sections in cooling channel test bench. (b): Local temperature profile in coolant domain.

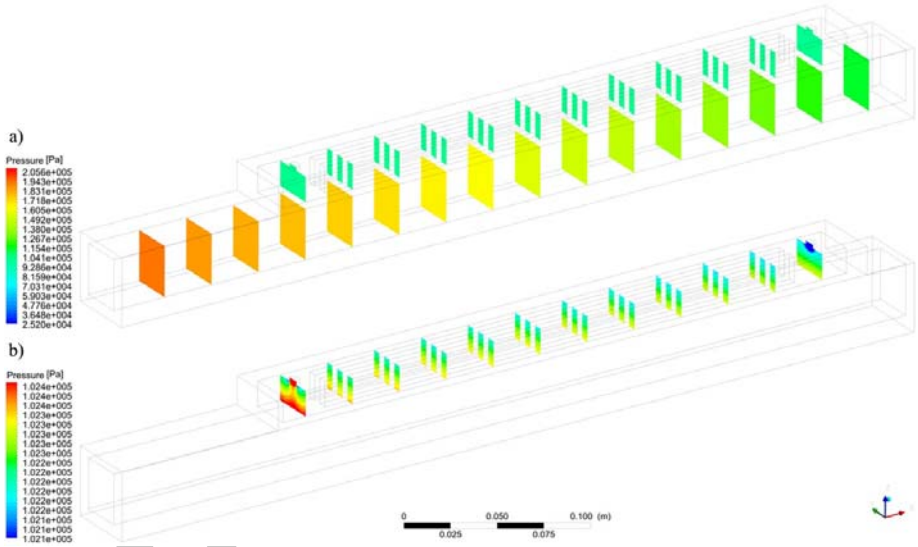

Fig. 15. (a): Global Pressure at various cross sections in coolant and combustion gas domain. (b): Local pressure at various cross sections in coolant domain.

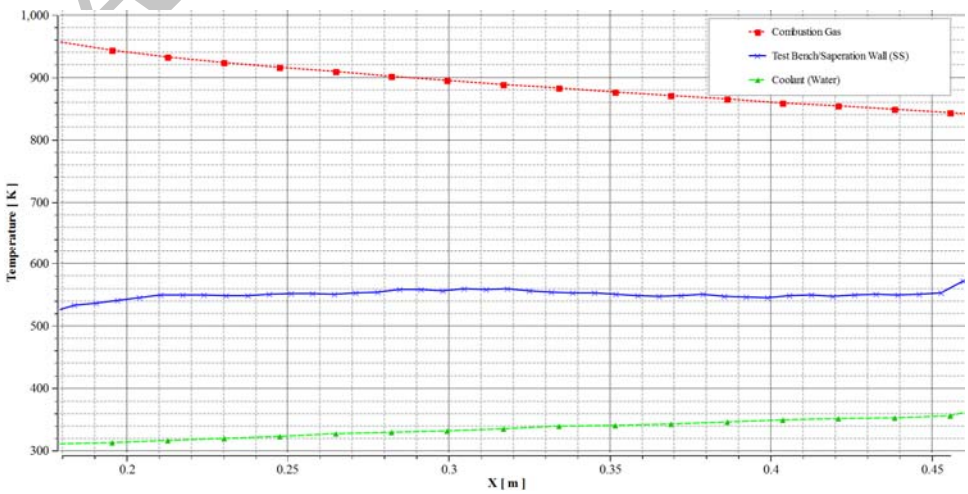

Fig. 16. Plot of temperature v/s location of coolant, cooling channel and combustion gas domain.

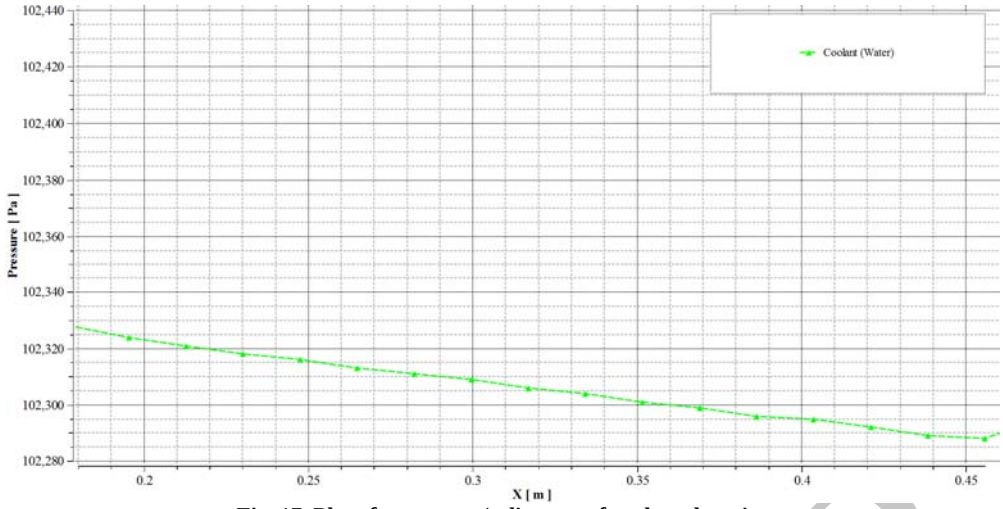

Fig. 17. Plot of pressure v/s distance of coolant domain.

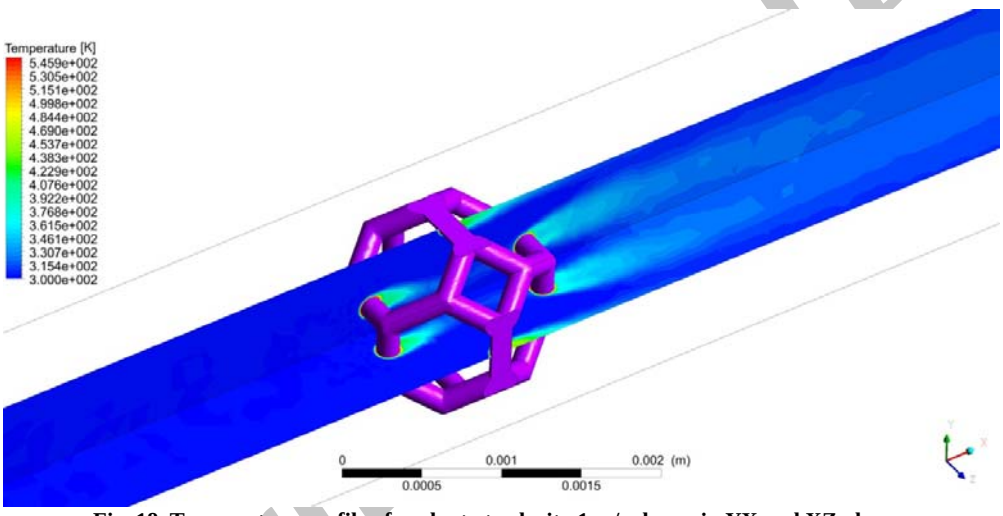

Fig. 18. Temperature profile of coolant at velocity 1 m/s shown in YX and XZ planes.

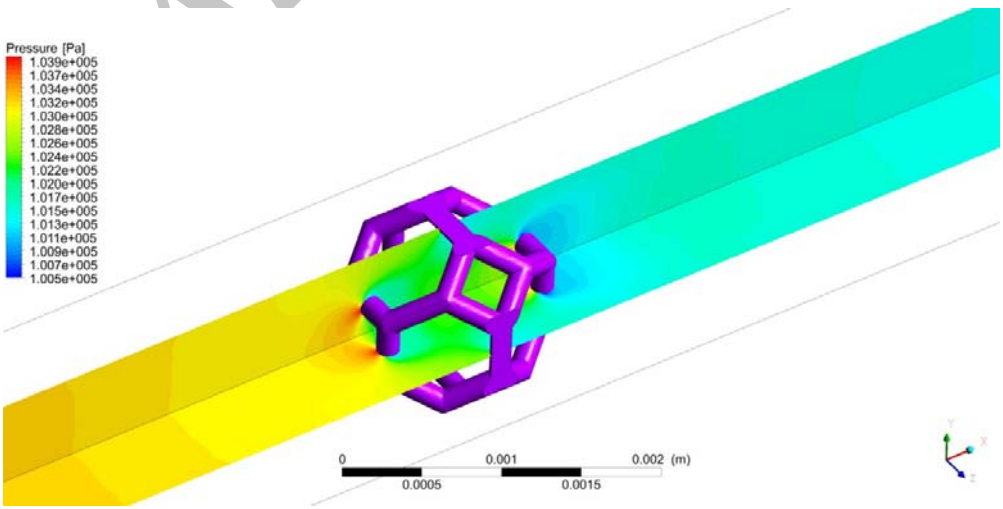

Fig. 19. Pressure in coolant at velocity 1 m/s shown in YX and XZ planes.

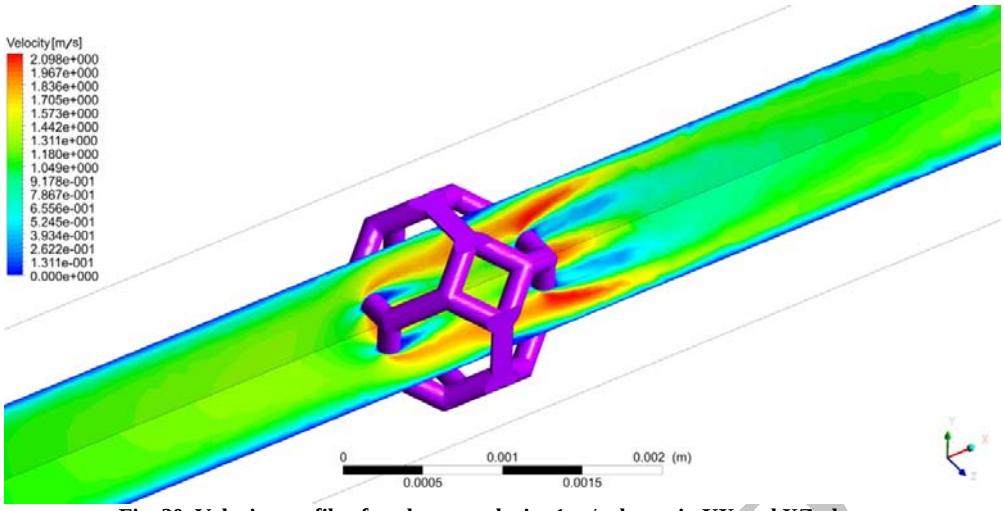

Fig. 20. Velocity profile of coolant at velocity 1 m/s shown in YX and XZ planes.

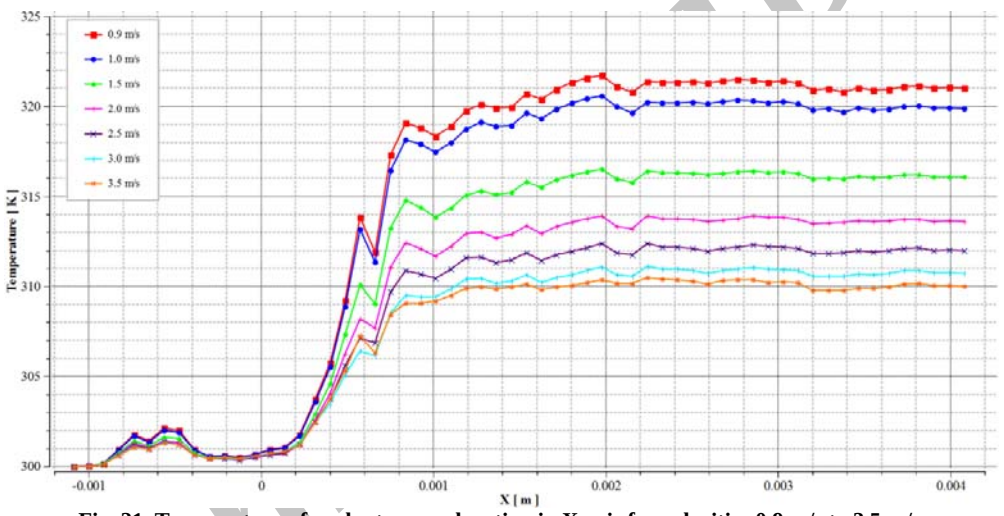

Fig. 21. Temperature of coolant versus location in X axis for velocities 0.9 m/s to 3.5 m/s.

different velocities (0.9 m/s, 1.0 m/s, 1.5 m/s, 2.0 m/s, 2.5 m/s, 3.0 m/s, 3.5 m/s). This rise in coolant temperature is because of the heat convection process from the TD unit cell. The final temperature distribution of the coolant at the outlet plane at different coolant flow velocities is presented in Fig 24. From the numerical analysis using CFD, it is observed that at 0.9 m/s of coolant flow velocity the overall temperature rise of the coolant is 20.916 K. In the same fashion, at 1.0 m/s it is 19.812 K, at 1.5 m/s it is 15.995 K, at 2.0 m/s it is 13.538 K, at 2.5 m/s it is 11.931 K, at 3.0 m/s it is 10.661 K and at 3.5 m/s it is 9.09 K respectively. Hence, it is evident that the overall coolant temperature rise decreases as the flow velocity of the coolant increases.

Fig. 22 shows pressure variations of the coolant as it passes thought the TD unit cell. It is observed that the pressure of the coolant increases as it approaches the unit cell and then abruptly decreases as the coolant enters into the unit cell followed by a gradual rise of the pressure before finally settling down to the ambient pressure at the outlet. The plot also concludes the fact that as the velocity of the coolant is higher, the steeper change in pressure occurs and it makes a way through and out of the copper foam. The Fig. 23 shows the total pressure of the coolant as it passes through the TD unit cell. It indicates an unexpected drop in total pressure of the coolant as it enters the TD unit cell and then remains almost constant throughout the reminder of the flow. The plot also highlights that, the higher the inlet velocity of the coolant the larger the drop in total pressure.

6. CONCLUSIONS

In the present article, the influence of a unit cell of copper metal foam in cooling channels to overall temperature rise of the coolant is numerically simulated using coupled CFD micro analysis. The results concluded its positive contribution to the overall coolant temperature rise without significant

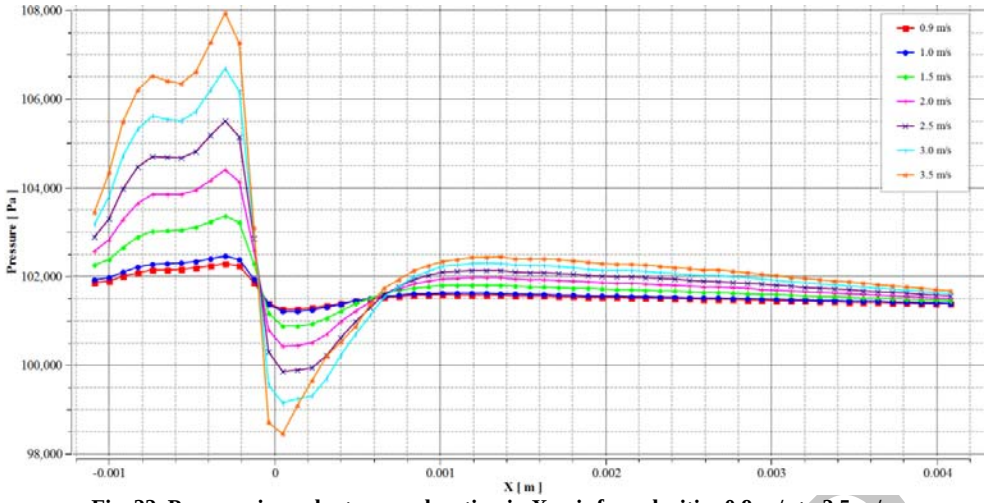

Fig. 22. Pressure in coolant versus location in X axis for velocities 0.9 m/s to 3.5 m/s.

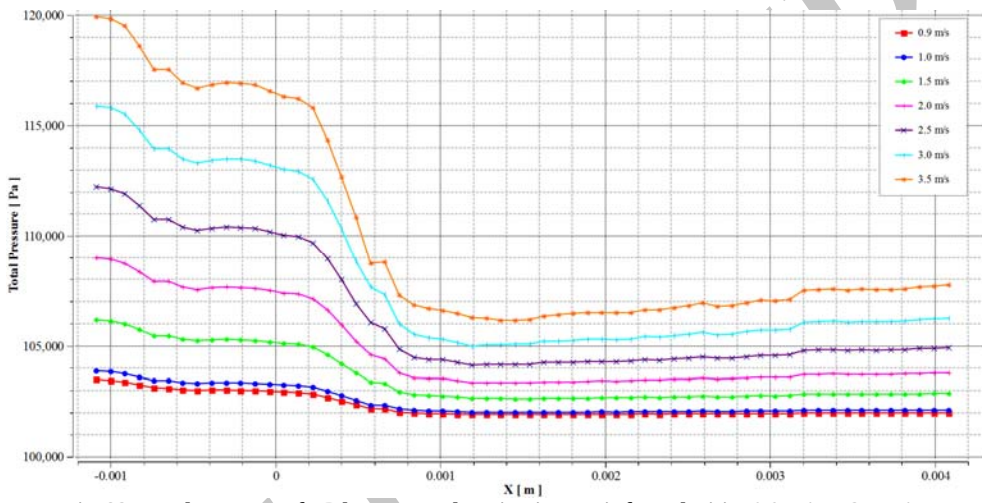

Fig. 23. Total pressure of coolant versus location in X axis for velocities 0.9 m/s to 3.5 m/s.

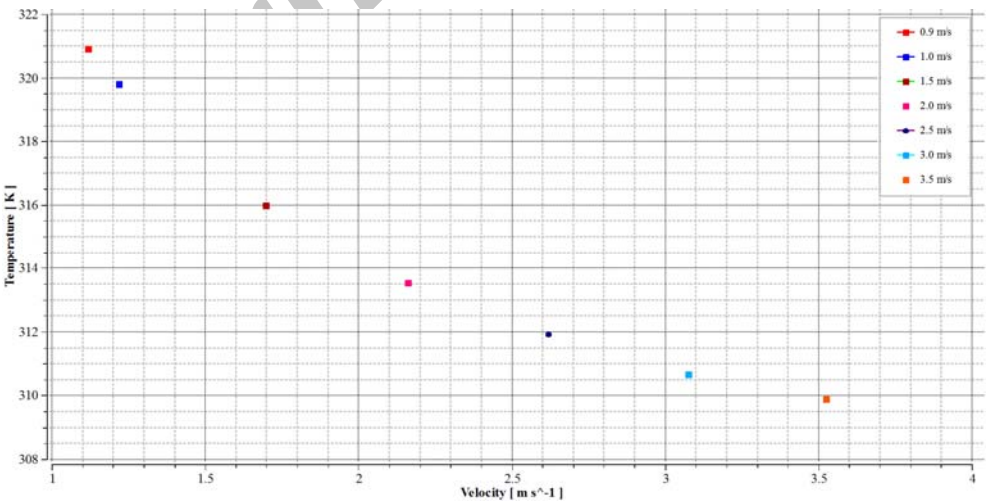

Fig. 24. Temperature of coolant at outlet plane for velocities 0.9 m/s to 3.5 m/s.

drop in pressure. In order to study the detailed effects of metal foam inserted in cooling channel on coolant temperature rise and pressure drop, the authors propose the fabrication of test bench with or without scaling. The initial test can be conducted using copper metal foam (50 ppi size) with water as

coolant and air-kerosene combustion gas as heat source to simulate the conditions relevant to liquid propulsion systems. Additionally, the investigation has revealed the fact that, as the inlet velocity of the coolant increases the overall coolant temperature decreases because of the metal foam inserts.

ACKNOWLEDGEMENT

The authors would like to express their gratitude to Mr. J. C. Pisharady, Division Head of Thermal Engineering Group, Liquid Propulsion System Centre for availing their facility to further experimental investigation in this matter. The author would also like to thank the significant contributions of Mr. A. Balasubramanian, Anna University, Dr. Rohan George Tharakan, University of Nottingham, Mr. S. Ajith, Lab Technician, Propulsion Software Validation Laboratory, LPSC, Mr. Renjith P. Nair and Mr. Lavish Ordia, Indian Institute of Technology, Mumbai towards this work.

REFERENCES

Bai M. and J. N. Chung (2011). Analytical and numerical prediction of heat transfer and pressure drop in open-cell metal foams. *International Journal of Thermal Sciences* 50(6), 869–880.

Boomsma, K. and D. Poulikakos (2001). The effects of compression and pore size variations on the liquid flow characteristics in metal foams. *ASME Journal of Fluids Engineering* 124, 263–272.

Boomsma, K. (2001). *Metal Foams as Novel Compact High Performance Heat Exchangers for the Cooling of Electronics*. Ph. D. thesis, Swiss Federal Institute of Technology, Zurich, Switzerland.

d'Arcy Thompson (1995). On Growth and Form, Canto, Cambridge 121.

Ding, X. R, L. S. Lu, C. Chen, Z. S. He and D. S. Ou(2011). Heat transfer enhancement by using four kinds of porous structures in a heat exchanger. *Applied Mechanics and Materials* 52–54, 1632–1637.

Hunt, M. L. and C. L. Tien (1988). Effects of thermal dispersion on forced convection in fibrous media. *International Journal of Heat and Mass Transfer* 31, 301–309.

Kherief, N. M., F. Berrahil and K. Talbi (2014). Magneto-Hydrodynamic Flow in a Two-Dimensional Inclined Rectangular Enclosure Heated and Cooled on Adjacent Walls. *Journal of Applied Fluid Mechanics* 9(1), 205-213.

Lebedev, A. B., A. N. Secundov, A. M. Starik, N. S. Titova and A. M. Schepin (2009). Modeling study of gas-turbine combustor emission In *proceedings of the Combustion Institute* 32 2941–2947.

Lu, W., C. Y. Zhao and S. A. Tassou (2006). Thermal analysis on metal-foam filled heat exchangers, Part I. Metal-foam filled pipes. *International Journal of Heat and Mass Transfer* 49, 2751–2761.

Mancin, S., C. Zilio, A. Diani and L. Rossetto (2012). Experimental air heat transfer and pressure drop through copper foams. *Experimental Thermal and Fluid Science* 36, 224–232.

Mancin, S., C. Zilio, L, Rossetto and A. Cavallini (2011). Heat transfer performance of aluminum foams. *Journal of Heat Transfer* 133(6).

Odabaee, M. and K. Hooman (2011). Application of metal foams in air-cooled condensers for geothermal power plants: an optimization study. *International Communications in Heat and Mass Transfer* 38(7), 838–843.

Odabaee, M. and K. Hooman (2012). Metal foam heat exchangers for heat transfer augmentation from a tube bank. *Applied Thermal Engineering* 36, 456–463.

Odabaee, M., K. Hooman and H. Gurgenci (2011). Metal foam heat exchangers for heat transfer augmentation from a cylinder in cross-flow. *Transport in Porous Media* 86(3), 911–923.

T'Joen, C., P. D. Jaeger, H. Huisseune, S. V. Herzeele, N. Vorst and M. D. Paepe (2010). Thermo-hydraulic study of a single row heat exchanger consisting of metal foam covered round tubes. *International Journal of Heat and Mass Transfer* 53, 3262–3274.

Thomson, W. (1887). On the division of space with minimum partitional area. *Philosophical Magazine* 5(24), 503-514.

Zhao, C. Y., T. Kim, T, J. Lu and H. P. Hodson (2002). Modelling on thermal transport in cellular metal foams. In: *8th Joint AIAA/ASME Thermophysics. Heat Transfer Conference*, St. Louis, Missouri, USA.

Zhao, C. Y., T. Kim, T. J. Lu and H. P. Hodson (2004). Thermal transport in high porosity cellular metal foams. *AIAA Journal of Thermophysics and Heat Transfer* 18, 309–317.

Zhao, C. Y., W. Lu and S. A. Tassou (2006). Thermal analysis on metal-foam filled heat exchangers, Part II. Tube heat exchangers. *International Journal of Heat and Mass Transfer* 49, 2762–2770.